Kinetic Characterization of Myosin Head Fragments with Long-Lived Myosin·ATP States†

A. L. Friedman,‡,⊥ M. A. Geeves,§ D. J. Manstein,|| and J. A. Spudich*,‡

Department of Biochemistry, Stanford University, Stanford, California 94305, Max-Planck-Institut für Molekulare Physiologie, Postfach 102644, D-44026 Dortmund, Germany, and Max-Planck-Institut für Medizinische Forschung, Jahnstrasse 29, D-69120 Heidelberg, Germany

Received December 23, 1997; Revised Manuscript Received April 22, 1998

ABSTRACT: We have separately expressed the *Dictyostelium discoideum* myosin II nonhydrolyzer point mutations E459V and E476K [Ruppel, K. M., and Spudich, J. A. (1996) *Mol. Biol. Cell 7*, 1123−1136] in the soluble myosin head fragment M761-1R [Anson et al. (1996) *EMBO J. 15*, 6069−6074] and performed transient kinetic analyses to characterize the ATPase cycles of the mutant proteins. While the mutations cause some changes in mantATP [2′(3′)-*O*-(*N*-methylanthraniloyl)-ATP] and mantADP binding, the most dramatic effect is on the hydrolysis step of the ATPase cycle, which is reduced by 4 (E476K) and 6 (E459V) orders of magnitude. Thus, both mutant myosin constructs do in fact catalyze ATP hydrolysis but have very long-lived myosin·ATP states. The E459V mutation allowed for a direct measurement of the ATP off rate constant from myosin, which was found to be 2×10^{-5} s^{-1}. Actin accelerated ATP release from this E459V construct by at least 100-fold. Additionally, we found that the affinity of the E476K construct for actin is significantly weaker than for the wild-type construct, while the E459V mutant interacts with actin normally. Their functional properties and the fact that they can be produced and purified in large amounts make the E476K and E459V constructs ideal tools to elucidate key structural features of the myosin ATPase cycle. These constructs should allow us to address important questions, including how binding of ATP to myosin heads results in a >3 order of magnitude reduction in actin affinity.

Myosin II is a filament-forming motor protein that has been found in virtually every eukaryote that has been examined; it will be referred to simply as myosin for the remainder of this communication. The interaction of myosin with actin filaments produces force and displacement in muscle contraction and is necessary for cytokinesis (*1*) and capping of cell surface receptors (*2*). The general mechanism by which actomyosin hydrolyzes ATP[1] has been elucidated (*3*−*5*). However, many of the key features of the chemo-structural cycle remain to be established. The crystal structure of myosin proteolytic subfragment 1 (S-1) revealed that S-1 could be described by two major domains (*6*). The actin and ATP binding regions are part of a globular domain commonly referred to as the catalytic domain. The second domain is a continuation of the catalytic domain into a long α-helix that is surrounded by two light chains. Growing evidence indicates that this light chain binding domain acts as a mechanical amplifier of the structural changes that occur in the catalytic domain (*7*−*12*). A number of chemostructural models predict part of the S-1 molecule undergoes an axial rotation relative to the filament axis. The forward axial rotation that leads to actin filament sliding is probably associated with the P_i release step. One problem in elucidating the structural states of myosin during the biochemical cycle has been the short lifetime of the intermediates. An increase of the lifetime of the ATP state should allow for a more detailed probing of the structural transition that accompanies ATP binding.

Ruppel et al. (*13*) demonstrated that when *Dictyostelium discoideum* myosin is expressed with any of the mutations, E459V, N464K, or E476K, the mutant myosins have ATPase rates that are below detection. Photo-cross-linking experiments showed that they were deficient in their ability to hydrolyze bound ATP (*13*). Thus, the myosin ATPase cycles of the mutants were dominated by the ATP-bound state. The mutations are within a highly conserved loop−helix region of myosin (*13*) which is roughly in the center of the catalytic domain. This region is apparently stabilized in at least two different positions that are dependent upon the state of the

† This work has been supported by NIH Grant UCSF/1650SC-01-A-3.

* To whom correspondence should be addressed.

‡ Stanford University.

⊥ Present address: Cellomics, Inc., 635 William Pitt Way, Pittsburgh, PA 15238.

§ Max-Planck-Institut, Dortmund.

|| Max-Planck-Institut, Heidelberg.

[1] Abbreviations: ATP, magnesium adenosine 5′-triphosphate; S-1, rabbit myosin II proteolytic subfragment 1; MHF, myosin head fragment; HEPES, *N*-(2-hydroxyethyl)piperazine-*N*′-2-ethanesulfonic acid; βME, 2-mercaptoethanol; TAME, N_α-*p*-tosyl-L-arginine methyl ester; TPCK, N_α-*p*-tosyl-L-lysine chloromethyl ketone; PMSF, phenylmethanesulfonyl fluoride; NTA, Ni^{2+}-nitrilotriacetic acid; F-actin, filamentous actin; G-actin, globular actin; SDS−PAGE, sodium dodecyl sulfate−polyacrylamide gel electrophoresis; EDTA, ethylenediaminetetraacetic acid; EGTA, ethylene glycol bis(β-aminoethyl ether)-*N*,*N*,*N*′,*N*′-tetraacetic acid; DTT, dithiothreitol; mant, 2′(3′)-*O*-(*N*-methylanthraniloyl); DEAE, diethylaminoethyl; ADP, adenosine 5′-diphosphate; P_i, inorganic phosphate; TLC, thin-layer chromatography; S1Dc, *Dictyostelium discoideum* myosin II motor domain; na, not applicable.

S0006-2960(97)03143-7 CCC: $15.00
Published on Web 06/17/1998

nucleotide that is bound to myosin. The loop is part of the nucleotide binding pocket in the structure of *D. discoideum* myosin catalytic domain complexed with ADP·vanadate (14), but is absent from this pocket in all other structures seen thus far (*15*−*17*). The residues of the loop may therefore be important for coupling nucleotide hydrolysis to conformational changes of the protein. Kinetic and detailed structural characterizations of the mutations require that they be expressed in soluble head fragments rather than full-length myosin because the latter forms filaments over a large range of salt concentrations (*18*) and cannot be crystallized.

Manstein and colleagues have engineered proteins consisting of the first 761 amino acids of the catalytic domain of *D. discoideum* myosin fused to 1 or 2 α-actinin repeats in place of the native light chain binding domain. They are called M761-1R and M761-2R with 1R and 2R referring to the number of α-actinin repeats. These fusion proteins have very similar kinetic rate constants to recombinant *D. discoideum* S-1 (which will be referred to as M864), propel actin filaments in vitro, form crystals, and can be expressed to levels of tens to hundreds of milligrams in the *D. discoideum* expression system (*11*, *19*). We expressed the nonhydrolyzer point mutations E476K and E459V separately in M761-1R. The new proteins will be referred as E476K and E459V for simplicity for the remainder of this communication.

Here we report detailed kinetic characterizations of the ATPase cycles of E476K and E459V and show that they have a 10^4- and 10^6-fold slowing of the ATP hydrolysis step, respectively. They therefore have myosin catalytic domains that do in fact catalyze ATP hydrolysis but have very long-lived myosin·ATP states. The stable E459V·ATP complex allowed for the measurement of the ATP off rate constant. We have also measured the general actin filament binding properties of E476K and E459V, and learned that E476K may be permanently in a low actin affinity state. E459V binds to and releases from actin filaments in an ATP-sensitive fashion, and may be an ideal reagent for the structural analysis of the myosin·ATP state.

MATERIALS AND METHODS

Protein Expression and Purification. Plasmids were constructed by cloning a fragment of a pBIGMyD-X/X nonhydrolyzer plasmid (*13*) into a vector derived from pDH12-1R which is a plasmid that contains the gene for the fusion protein M761-1R (*11*). Specifically, nonhydrolyzer pBIGMyD-X/X and pDH12-1R were digested with the endonucleases *Eco*NI and *Bbs*I which have unique sites in pDH12-1R. The pDH12-1R vector was treated with phosphatase and ligated with the appropriate pBIG-derived fragment. The fidelity of the resulting plasmids was checked through diagnostic digests and dideoxy-sequencing. pAF3 and pAF4 contain the genes for E476K and E459V, respectively. *D. discoideum* orf^+ cells were transformed through electroporation and then grown at 22 °C in broth containing (units are g/l) 20 protease peptone (Oxoid), 7 yeast extract (Oxoid), 8 glucose, 0.47 $Na_2HPO_4{\cdot}7H_2O$, and 0.35 KH_2PO_4. Selection and maintenance of cell lines were achieved with 15 μg/mL G418 (Gibco), and expression was checked through Western analysis (below). Plasmid DNA was rescued (Wizard Plus Minipreps; Promega) from the transformed *D. discoideum* and sequenced to check fidelity (ABI PRISM Dye Terminator Cycle Sequencing Ready Reaction Kit; Perkin-Elmer).

M761-2R, E476K, and E459V end in a C-terminal affinity tag consisting of eight His residues. M761-2R was purified via the methods described by Manstein and Hunt (*20*). E476K and E459V were purified in a similar fashion except that the first supernatant was applied directly to a nickel column and the eluted protein was further purified through gel filtration. Specifically 20−40 g of cells was grown, harvested, washed with phosphate-buffered saline, and resuspended in 4 mL of lysis buffer (50 mM HEPES, 5 mM benzamidine, 0.02% sodium azide, 7 mM βME, pH 8.0) per gram of cells, and ∼5 mm diameter pellets were rapidly frozen in liquid nitrogen for storage at −80 °C. A typical preparation began with the thawing, and therefore the lysing, of 20 g of cells to which the following were added: 2 mL of lysis buffer per gram of cells, 100 units of alkaline phosphatase, 15 μg/mL RNase, and protease inhibitors (units are μg/mL; 100 TAME, 80 TPCK, 2 pepstatin, 5 leupeptin, 40 PMSF). The lysed cells were centrifuged (158000*g*, 1 h), and the majority of the mutant myosin fragment appeared in the supernatant (Figure 1, lane 5). A Waters 650E system was used to load and wash two columns. The supernatant was loaded at 1 mL/min onto a Ni^{2+}-NTA affinity column (0.7 × 11.5 cm) (Qiagen), and the column was washed with low-salt buffer (50 mM HEPES, 30 mM KOAc, 1 mM benzamidine, 7 mM βME, pH 7.4), high-salt buffer (low-salt buffer plus 270 mM KOAc), and low-salt buffer containing 50 mM imidazole. A linear gradient of low-salt buffer and imidazole buffer (500 mM imidazole, 1 mM benzamidine, pH 7.4) was used to elute the protein. Column fractions were analyzed with SDS−PAGE and pooled based on yield and purity. The sample was then dialyzed overnight at 4 °C versus concentrating buffer (25% sucrose, 20 mM HEPES, 0.5 mM EDTA, 0.5 mM EGTA, 1 mM DTT, 1 mM benzamidine) which reduced the volume by 50−75%. The protein was then gel-purified with a Pharmacia HiLoad 16/60 Superdex 200 column which had been equilibrated with experimental buffer (25 mM HEPES, 100 mM KCl, 5 mM $MgCl_2$, 5 mM βME; pH 7.0 at 20 °C). The typical yield and concentration of purified protein were 5 mg and 5 μM, respectively. The purity of a typical preparation is demonstrated in Figure 1 (lane 7). A Centriprep 30 (Amicon) was used to further concentrate the protein for the acid quench experiments.

The very slow rate of ATP hydrolysis of E459V (Results) made necessary an unusual step in myosin protein purification to remove bound ATP from the purified E459V. The preparation was dialyzed versus 1 L of modified experimental buffer (1 mM EDTA and 20 mL of bagged DEAE resin were added, and no $MgCl_2$ was present) at 20−24 °C for 2−3 days with daily buffer changes. To check the progress of the evolution of the nucleotide-free form of E459V, a sample of protein was removed at various times during the dialysis, and the fluorescence enhancement was measured on adding protein to mantATP.

Stopped-Flow and Fluorimetry Experiments. Fluorimetry experiments were performed with an SLM AB2 fluorimeter with excitation/emission bandwidths set at 4 nm. Mant fluorescence was excited and collected at 355 and 440 nm, respectively; pyrene at 365 and 405 nm. Experimental

volumes were typically 700 μL. An addition of solution, mixing, and pause in data acquisition at an arrow in Figures 3, 5, and 6 occupied ~20 s. Stopped-flow experiments were performed with Applied Photophysics DX-17MV and Hi-tech Scientific SF-61MX systems. The mant derivatives of ATP and ADP were excited at 355 nm, pyrene was excited at 365 nm, and the emitted light passed through a KV 380 nm cutoff filter. Tryptophan fluorescence was excited at 295 nm, and emitted light was filtered through a SWG 305 nm cutoff filter. The reported concentrations refer to post-mixing in the experimental chamber. The buffer that was used for all fluorimetry, stopped-flow, acid quench, and cosedimentation experiments was the experimental buffer described above.

Proteins and Reagents. Rabbit skeletal muscle actin was purified by the method of Pardee and Spudich (*21*) and labeled with pyrene essentially by the method of Criddle et al. (*22*). The concentration measurement of pyrene-actin included a correction for absorbance of the label at 280 nm [A_{280} (pyrene) = 1.06 × A_{344} (*22*)]. Exogenous ATP was removed from F-actin by centrifugation directly before an experiment. The mant derivatives of ATP and ADP were prepared by reaction with *N*-methylisatoic anhydride as described by Hiratsuka (*23*), except that after reaction it was purified on a DEAE-cellulose column as described by Woodward et al. (*24*). Protein concentrations were determined by the absorbance at 280 nm and the following extinction coefficients (1 mg/mL, 280 nm) and molecular masses: 0.73 cm^{-1} and 103 kDa for E476K and E459V; 0.79 cm and 116 kDa for M761-2R; 1.15 cm^{-1} and 42 kDa for actin.

Electrophoretic Methods. SDS−PAGE and Western blot analyses were performed using standard conditions. Whole cell lysates for expression level screening were prepared by resuspending cells in lysis buffer with protease inhibitors (above) and 1% Triton. The transferred protein was probed with the myosin catalytic domain-specific monoclonal antibody M2.42 (kindly provided by Dr. Thomas D. Pollard) and a horseradish peroxidase-coupled secondary antibody (Biorad). An enhanced chemiluminescence system (Amersham Life Science) detected the secondary antibody.

Acid-Quench Experiments. Protein (16−25 μM) and mantATP were mixed in a 5:4 ratio and incubated at 20−24 °C. Samples were taken at different time points, and the reaction was quenched with 10% trichloroacetic acid. The samples were then centrifuged at 4 °C at 14 000 rpm for 30 min in an Eppendorf 5415C centrifuge. Aliquots of the supernatants were applied to fluorescent thin-layer chromatography plates (silica gel 60F 254 nm) and run with a 6:3:1 mixture of 1-propanol, ammonium hydroxide (30%), and water. The plates were analyzed by excitation at 365 nm, conversion of the plate image to a TIF file (IS-1000 Digital Imaging System, Alpha Innotech Corp., San Leandro, CA), and intensity measurements with Metamorph software (Universal Imaging Corp., Westchester, PA).

Actin Cosedimentation. A 4 μM sample of rabbit skeletal muscle actin was incubated on ice for 10 min with 4 μM purified E476K or M761-2R in experimental buffer. The sample was then centrifuged at 300000*g* for 30 min. The supernatant was removed, and a volume of fresh experimental buffer, equal to the supernatant volume, was used to resuspend the pellet. Supernatant and pellet samples were analyzed with SDS−PAGE, and quantitative analysis of Coomassie blue stained protein bands was performed with Metamorph. The gel sample volumes were chosen to yield stained bands that fell on the linear region of the stain/protein curve.

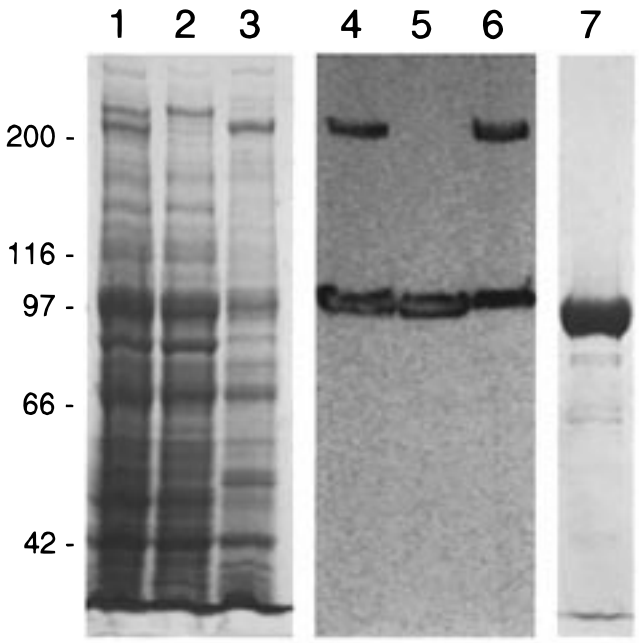

FIGURE 1: SDS−PAGE and Western blot analyses of samples from a typical purification of E459V. Lanes 1−3: SDS−PAGE of Coomassie blue stained whole cell lysate (1), and supernatant (2) and pellet (3) after the centrifugation step (Materials and Methods). Lanes 4−5: Western blot of the same samples as in panel A. Centrifugation removed the full-length myosin (~200 kDa). Lane 7: purified E459V overloaded to demonstrate the level of purity. E476K purifications gave similar results.

Data Analysis. Averages of one to three consecutive stopped-flow traces were analyzed with software that accompanies the Applied Photophysics device. Scatter plots (Figures 2B, 3C, 3D, 4, 5B, and 6B) were made with Kaleidagraph (Abelbeck Software) and fits made with the general curve-fitting feature of the software which uses the Levenberg−Marquardt algorithm. Error values in Table 1 and results are those reported by the Kaleidagraph software from a fit to a typical scatter plot.

RESULTS

The purification of myosin head fragments (MHFs) from *D. discoideum* has been described (*20*) but needed some modification before the nonhydrolyzer MHFs could be purified. In the published protocol, the cells are lysed, and ATP concentration is reduced. This causes wild-type MHFs to bind to cytoskeletal actin filaments and therefore pellet after centrifugation at 160000*g*. By contrast, immunoblots revealed that E476K and E459V remained mostly in the supernatant (Figure 1, lane 5; ~100 kDa mass). The protein was purified from the supernatant through Ni^{2+} affinity and sizing columns (Materials and Methods), and a typical sample appears in Figure 1, lane 7. The 200 kDa protein in lanes 4 and 6 is wild-type full-length myosin heavy chain which is completely removed during the first centrifugation (lane 5). Approximately 3 days of dialysis were required to remove all nucleotide from E459V. We chose to express E476K and E459V in cells expressing wild-type myosin because

Table 1: Kinetic Constants for MHFs in the Absence of Actin[a]

	M864[b]	M761-2R	E476K	E459V
k_{on}, mantADP (M^{-1} s^{-1})	9×10^5	$(7.9 \pm 2.2) \times 10^5$	$(5.3 \pm 0.8) \times 10^5$	$(1.1 \pm 0.2) \times 10^5$
k_{off}, mantADP (s^{-1})	1.5	1.5 ± 0.1	$(1.6 \pm 0.1) \times 10^{-1}$	$(5.4 \pm 0.1) \times 10^{-2}$
K_d, mantADP (μM)[c]	1.7	1.9	0.3	0.5
k_{on}, mantATP (M^{-1} s^{-1})	7×10^5	$(2.9 \pm 0.7) \times 10^5$	$(3.6 \pm 0.2) \times 10^5$	$(0.76 \pm 0.14) \times 10^5$
k_{off}, mantATP (s^{-1})	na	na	na	2×10^{-5}
K_d, mantATP (nM)[c]	na	na	na	0.3
hydrolysis (s^{-1})	24	27 ± 1	$(1.2 \pm 0.1) \times 10^{-3}$	$(5.9 \pm 1.4) \times 10^{-5}$

[a] Conditions: 25 mM HEPES, 100 mM KCl, 5 mM $MgCl_2$, 5 mM βME, pH 7.0. [b] Ritchie et al. (1993) (*25*). [c] Calculated from k_{off}/k_{on}.

wild-type cells grow in suspension culture whereas cells lacking myosin must be grown on surfaces. M761-1R and M761-2R have nearly identical kinetic rate constants (*19*), and M761-2R was used as the wild-type control in all experiments presented in this communication.

On and Off Rate Constants for Nucleotide Binding. Point mutations may cause changes in any of the rate constants of the ATPase cycle. It is therefore important to determine which kinetic steps may be altered and by how much. *D. discoideum* myosin head fragments do not change their intrinsic fluorescence when nucleotide binds, but the rates of nucleotide binding can be measured by using the fluorescent analogue mantATP (*25*, *19*). A typical reaction observed on adding 1.3 μM mantADP to 0.25 μM E476K is shown in Figure 2A with a fit of a single-exponential function to the data. The observed rate constant (k_{obs}) was plotted versus nucleotide concentration, and the data could be described by a straight line. The slopes of linear fits to the data points defined the second-order rate constant of mantADP binding. Similar data were collected for M761-2R and E459V with both mantADP and mantATP, and the data are summarized in Figure 2B and Table 1. The mantATP on rate constants for both mutants and the mantADP on rate constant for E476K showed little change relative to the rate constants obtained with the M761-2R wild-type construct. However, the mantADP on rate constant for E459V was reduced by an order of magnitude. The mantADP off rate constant was measured by incubating 0.4 μM mantADP with 0.5 μM E476K, E459V, or M761-2R and using the stopped-flow device to rapidly mix 200 μM unlabeled ATP with the complex. The resulting decay in fluorescence could be described by a single-exponential function whose rate constant was taken as the mantADP off rate constant. This parameter was reduced by about 1 order of magnitude in the mutants. The ratios of the dissociation and association rate constants (k_{off}/k_{on}) define K_d for ligand binding and are given in Table 1. The values are similar for the three constructs at 1.9 μM, 0.3 μM, and 0.5 μM for M761-2R, E476K, and E459V, respectively.

Hydrolysis Rate Constants. Ritchie et al. (25) demonstrated that ATP binding does not cause an intrinsic fluorescence increase in *D. discoideum* S-1, as it does for rabbit S-1. However, the hydrolysis step in the *D. discoideum* S-1 ATPase cycle is associated with an intrinsic fluorescence increase. The rate of the hydrolysis step of M761-2R was measured by Kurzawa et al. (32 s^{-1}; ref *19*) using this change in fluorescence. This experiment was repeated and gave a very similar result, 27 s^{-1} (Table 1). E476K and E459V failed to show any change in intrinsic protein fluorescence on the tens of seconds time-scale when mixed with ATP. This is consistent with the absence of a change of fluorescence upon binding and a very slow hydrolysis step relative to M761-2R.

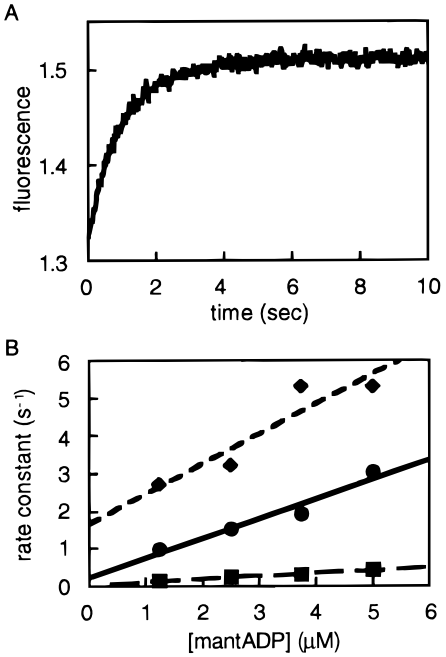

FIGURE 2: MantADP on rate constants. Typical stopped-flow trace, with fit, and second-order rate constant measurements. (A) An average of three consecutive traces obtained by mixing 1.25 μM mantADP with 0.25 μM E476K. The observed rate constant of the reaction was 0.96 s^{-1}. (B) Observed rate constant versus [mantADP] for M761-2R (◆), E476K (●), and E459V (■). The slopes of the fits are the second-order rate constants of mantADP binding and are listed in Table 1. Conditions for Figures 2−6: 25 mM HEPES, 100 mM KCl, 5 mM $MgCl_2$, 5 mM βME; pH 7.0. The temperature for the experiments in Figures 2, 3, 5, and 6 was 20 °C.

The rates of the hydrolysis step of the mutants were measured by performing single mantATP turnover experiments. Adding 1.25 molar excess of either mutant to mantATP caused a fluorescence enhancement which showed saturation at concentrations above 0.2 μM. These control experiments indicated that the affinity of mantATP was $\ll$0.2 μM, and thus essentially all of the mantATP was bound at concentrations above this value. Figure 3A shows the increase in the fluorescence of 0.4 μM mantATP on adding 0.5 μM E476K (filled arrow, upper trace). Following the rise in fluorescence, which indicated the formation of the mantATP·E476K complex, the signal decreased slowly as the mantATP was hydrolyzed, and P_i and mantADP were subsequently released. A significant fraction of mantADP remained bound to the protein at the end of the reaction because the K_d is 0.3 μM (Table 1). To prevent mantADP rebinding, 200 μM unlabeled ATP was added at the unfilled arrow. The signal dropped rapidly by a small fraction,

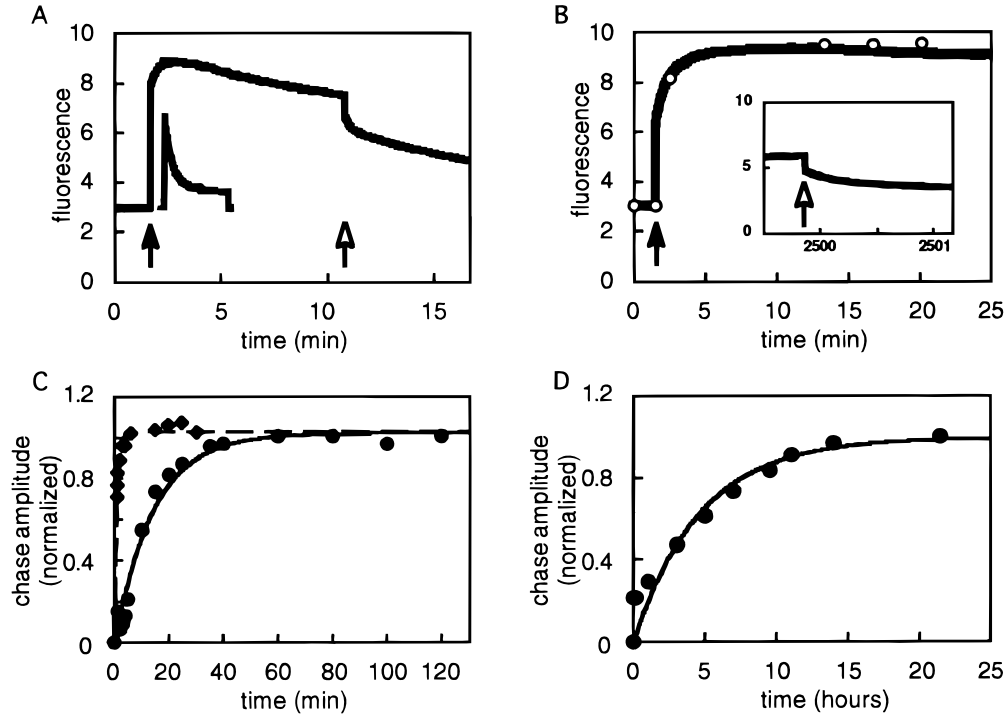

FIGURE 3: Single mantATP turnover experiments with E476K, E459V, or M761-2R. (A) 0.5 μM E476K was added to 0.4 μM mantATP at the filled arrow (upper trace), and 200 μM unlabeled ATP at the unfilled arrow. Data were corrected for dilution. The same experiment was performed with M761-2R (lower trace in panel A) and E459V (panel B). In panel B, the open circles are data points collected when the excitation shutter was opened briefly, which demonstrated that the slow decrease in signal ($t = 10-25$ min) was due to photobleaching. (Inset) Addition of the unlabeled ATP after incubation of the E459V·mantATP solution for 1.7 days. (C) The amplitude of the fast phase of the signal decrease, after the addition of the unlabeled ATP, plotted versus time for M761-2R (◆) and E476K (●). (D) A repeat of the previous experiment with E459V. k_{obs} was 1.2×10^{-3} s^{-1} and 5.9×10^{-5} s^{-1} for E476K and E459V (Table 1).

indicating displacement of bound mantADP, before returning to the slow rate of decay. The rates of decrease of the signal at 8 and 15 min are similar because both are limited by the actual hydrolysis step of the ATPase cycle. The single mantATP turnover experiment for M761-2R is also shown in Figure 3A (lower trace); 0.5 μM M761-2R was added to 0.4 μM mantATP, and bound quickly which resulted in a rapid rise in fluorescence. The signal returned to close to the initial level within 5 min as the ATP was hydrolyzed and P_i and mantADP were released. Complete return to the base line required addition of unlabeled ATP to displace the small amount of mantADP that remained bound to the protein at the end of the reaction. E459V was also characterized in this way but did not show any decline in signal on the minutes time-scale (Figure 3B). The very slow decrease in signal for E459V ($t = 10-25$ min) was due to photobleaching; when the dye molecules were excited for only 10 s per data point (open circles), the slow decrease was eliminated. When the E459V/mantATP sample was incubated for greater than 1 day, the release of bound mantADP was detected by again chasing with 200 μM unlabeled ATP (inset). The signal returned to base line which indicated that E459V had completely hydrolyzed the mantATP within 1 day.

If the rapid signal changes at the open arrows in panels 3A and 3B were due to displacement of the protein-bound mantADP by the excess ATP, then the amplitude of these signal changes should have increased with the time of incubation of the mantATP and the protein (e.g., time between closed and open arrows in panel 3A). To examine this, we preincubated 0.4 μM mantATP with 0.5 μM of one of the proteins, and then used a stopped-flow device to rapidly add the 200 μM unlabeled ATP and record the subsequent decay in fluorescence at different times after the addition of unlabeled ATP. For E476K, the signal decreased in two phases, consistent with the signal decrease seen in Figure 3A (open arrow). A double-exponential function was fit to the signal, and the observed rate constants of the faster and slower phases were 0.18 ± 0.03 s^{-1} and 0.021 ± 0.002 s^{-1} (mean $\pm$ sem; $n = 15$), respectively. The slow phase is thought to be dominated by photobleaching because of the intense light source used in the stopped-flow device. The observed rate constant of the faster phase was similar to the rate constant of mantADP release (0.16 s^{-1}; Table 1) as expected. The amplitude of the faster phase increased with time and followed a time course that was well described by a single exponential with a k_{obs} of 1.2×10^{-3} s^{-1} (Figure 3C, circles; Table 1). When the same experiments were performed with M761-2R and E459V, the turnover rates were 1.5×10^{-2} s^{-1} (Figure 3C, diamonds) and 5.9×10^{-5} s^{-1} (Figure 3D; Table 1). The turnover rate of E476K could be reduced ~4-fold by lowering the temperature from 20 to 4 °C.

Direct measurements of evolved mantADP demonstrated that the single-turnover rates of E476K and E459V were controlled by the hydrolysis step. The evolution of bound and free mantADP was measured by simply acid-quenching the reaction instead of chasing with unlabeled ATP. The concentrations of mantATP/ADP at each time point were measured by TLC and plotted versus time (Figure 4A,B). The rate constants of the reactions were 2×10^{-3} s^{-1} and 6×10^{-5} s^{-1} for E476K and E459V, respectively, which are in general agreement with the results from the stopped-flow experiments (Figure 3C,D, Table 1). The consumption of mantATP by M761-2R was complete within the earliest time

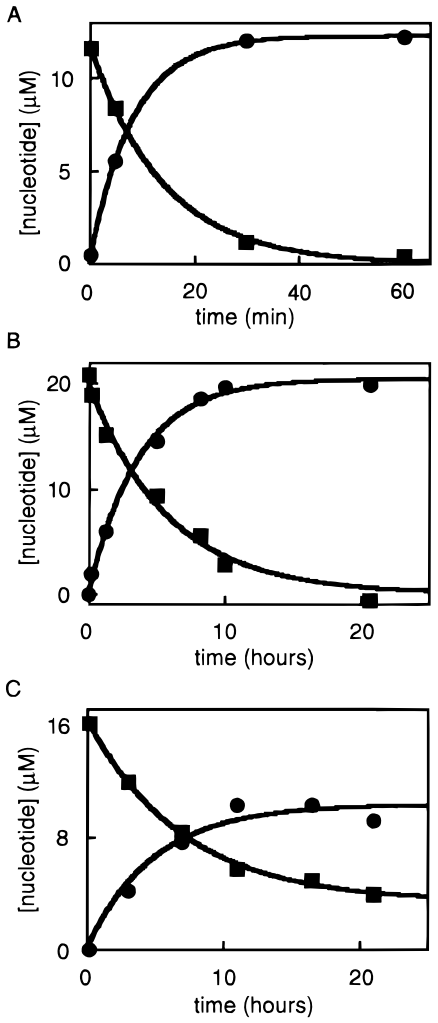

FIGURE 4: TLC measurements of the concentrations of the total mant nucleotide, after acid quench, from single-turnover experiments at 20−24 °C. Panel A: 16 μM E476K; k_{obs} values for the mantADP (●) and mantATP (■) fits were 2.0×10^{-3} s^{-1} and 1.2×10^{-3} s^{-1}. Panel B: 25 μM E459V; 7.5×10^{-5} s^{-1} (●) and 4.7×10^{-5} s^{-1} (■). Panel C: Measurement of the mantATP off rate constant by repetition of the E459V experiment (Figure 4B) with 2 mM unlabeled ATP added 10 min after the mantATP addition. The fits to the mantADP (●) and mantATP (■) data gave k_{obs} of 6.0×10^{-5} s^{-1} and 3.9×10^{-5} s^{-1}, with amplitudes of 10 μM and 13 μM, respectively.

point (30 s) of the acid quench experiments. This result is consistent with the hydrolysis rate constant of 27 s^{-1} measured by the intrinsic fluorescence change (above).

MantATP Off Rate Constant for E459V. The extremely slow rate of the hydrolysis step of E459V allowed for the use of the "cold-chase" approach (*26*, *27*) to directly measure the mantATP off rate constant from E459V. The E459V quench experiment (Figure 4B) was repeated in the presence of 2 mM unlabeled ATP (Figure 4C), which was added 10 min after the protein was mixed with the mantATP. After 21 h, by which time all of the mantATP in control experiments was completely hydrolyzed (Figure 4B), the mantATP:mantADP ratio was 0.33 (Figure 4C). This result demonstrated that unlabeled ATP displaced about one-third of the bound mantATP. The experiment was repeated without protein, and <5% of the mantATP was hydrolyzed within 21 h. The data were analyzed in terms of Scheme 1 where M·ATP breaks down irreversibly along two pathways: backward to the nucleotide-free state (determined by the mantATP off rate constant, k_1), or forward to the M·products state (determined by the hydrolysis rate constant, k_2).

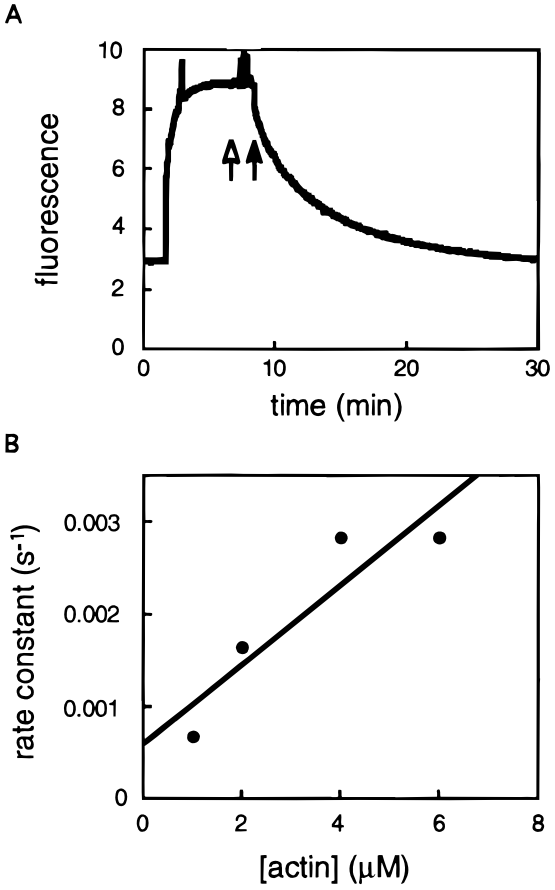

FIGURE 5: Actin-induced release of mantATP from E459V. (A) 0.5 μM E459V was added to 0.4 μM mantATP at $t = 1.7$ min, 200 μM unlabeled ATP at the unfilled arrow, and 4 μM actin at the filled arrow. The decrease in signal following actin addition was well-described by a single exponential; $k_{obs} = 0.0028$ s^{-1}. (B) Dependence of the observed rate constant on actin concentration. The slope of the fit is $(4 \pm 1) \times 10^2$ M^{-1} s^{-1} and defines the apparent second-order rate constant for the actin-induced dissociation of mantATP.

Scheme 1

$$\mathrm{M} + \mathrm{ATP} \overset{k_1}{\longleftarrow} \mathrm{M{\cdot}ATP} \overset{k_2}{\longrightarrow} \mathrm{M{\cdot}products}$$

An ATP binding step does not exist because unlabeled ATP prevents rebinding of mantATP. One feature of the model is that the mantATP off rate constant (k_1) can be calculated by multiplying the final mantATP:mantADP ratio (3.3 μM/10 μM) by the E459V hydrolysis rate constant (k_2; 5.9×10^{-5} s^{-1}, Table 1). Thus, the mantATP off rate constant from E459V is 2×10^{-5} s^{-1} (Table 1).

A further important question that was addressed with E459V was whether actin accelerates the ATP off rate constant. The experiment of Figure 3B was repeated with an inclusion of a 1−6 μM actin addition step. Figure 5A shows that 0.4 μM E459V·mantATP complex was again formed, but now a large excess of unlabeled ATP was added to ensure that the released mantATP would not rebind (open arrow). Following actin addition (filled arrow), the fluo-

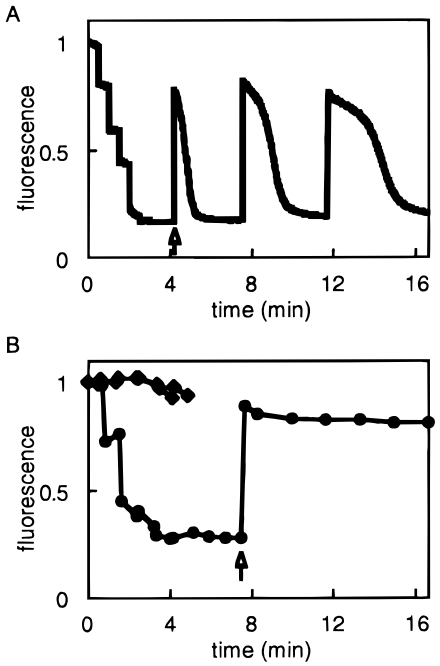

FIGURE 6: Interaction of M761-2R, E476K, and E459V with pyrene-labeled actin filaments. (A) 1.5 μL of 103 μM M761-2R was added to 700 μL of 0.8 μM pyrene-actin at $t = 0.5$, 1.0, 1.5, 2.0, 2.5, and 3.0 min. 5, 10, or 15 μM ATP was added at $t = 4.2$, 7.5, or 11.8 min, respectively. (B) Repetitions of the experiment with E476K (◆) and E459V (●), with the samples protected from the excitation radiation between data points. 5 μL of 54 μM E476K was added at $t = 0.7$, 1.5, 2.5, and 3.5 min. 5 μM ATP was added at $t = 4.2$ min. 25 μL of 7.7 μM E459V was added at $t = 0.8$, 1.6, 2.5, 3.3, and 4.1 min. 5 μM ATP was added at $t = 7.5$ min. E476K and E459V data points were corrected for dilution.

rescence signal decreased to base line and was well described by a single-exponential function. A plot of k_{obs} versus actin concentration is shown in Figure 5B. Analysis of the products of the reaction by TLC showed no evidence of mantATP hydrolysis on the time scale of the fluorescence change. Thus, the fluorescence change represents the displacement of mantATP from E459V by actin with no evidence of any acceleration of the ATP cleavage step by actin. The slope of the line in Figure 5B defines the apparent second-order rate constant for the actin-induced dissociation of mantATP and is $(4 \pm 1) \times 10^2$ M^{-1} s^{-1}.

Actin Binding. The interaction of E476K and E459V with actin was further investigated by measuring binding and release from pyrene-labeled actin filaments. The fluorescence of *N*-(1-pyrene)iodoacetamide covalently bound to cysteine-374 of actin is mostly quenched when rabbit S-1, M864, or M761-2R binds to the actin (*28*, *25*, *19*). Figure 6A shows the fluorescence of 700 μL of 0.8 μM pyrene-actin to which 1.5 μL aliquots of 103 μM M761-2R were added until the fluorescence was fully quenched, which indicated the occupation of available myosin binding sites. 5 μM ATP was then added to the reaction, and the signal rapidly increased as M761-2R dissociated from actin (unfilled arrow at $t = 4.2$ min). The pyrene signal was again quenched when the complex re-formed after the ATP was fully hydrolyzed ($t = 6$ min). When 10 or 15 μM excess ATP was added ($t = 7.5$ or 11.8 min), the amount of time necessary for the protein to fully rebind to actin increased proportionally. When the same experiment was repeated with E459V (Figure 6B, circles), the pyrene signal was quenched in a fashion similar to the M761-2R experiment. When the 5 μM excess ATP was added (unfilled arrow), E459V released rapidly from pyrene-actin but did not rebind on the minutes time-scale. This result was consistent with a very long-lived myosin·ATP state. The protocols used for the experiments presented in panels A and B differ only in that photobleaching was minimized by closing the excitation shutter between acquisition of data points (circles) in panel B.

The relationship between ATP concentration and the rate of release from pyrene-actin filaments (Figure 6; open arrows) was investigated with a stopped-flow device (*25*). The fluorescence signal was well-described by a single exponential, and the observed rate constant was linearly dependent on ATP concentration over a range of 10−40 μM ATP. The slopes of linear fits to the data points defined a second-order rate constant which was about an order of magnitude higher for E459V [$(1.4 \pm 1) \times 10^6$ M^{-1} s^{-1}] relative to M761-2R [$(0.41 \pm 0.03) \times 10^5$ M^{-1} s^{-1}].

When the actin binding protocol was repeated with E476K preparations, additions of E476K caused no detectable decreases in the fluorescence signal (Figure 6B, diamonds). Adding ATP after the E476K had no effect on the signal. The activities of the E476K preparations were checked by performing single-turnover experiments with the fluorimeter, and the results were the same as those presented in Figure 3A; the 3-fold increase in mantATP fluorescence (Figure 3A) demonstrated that the protein was nucleotide-free after purification. The inability of E476K to bind strongly to actin was confirmed by cosedimentation of 4 μM E476K and 4 μM actin. Less than 14% of the E476K appeared in the pellet when incubated with unlabeled actin in the absence of nucleotide and centrifuged at 300000*g*. Cosedimentation experiments with M761-2R confirmed that the actin preparation was able to bind myosin normally. The DNA that codes for the catalytic domain of E476K was sequenced, and as expected, no additional mutations were present. Thus, E476K may not interact strongly with actin in the absence of nucleotide.

DISCUSSION

Hydrolysis Rate Constants. The rates of the hydrolysis steps for E476K and E459V were obtained from the single-turnover experiments and found to be 1.2×10^{-3} s^{-1} and 5.9×10^{-5} s^{-1}. Intrinsic fluorescence was used to measure the rate of the hydrolysis step for M761-2R which yielded a value of 27 s^{-1} as seen in previous measurements (*19*). Thus, the hydrolysis steps of E476K and E459V are reduced by 4 and 6 orders of magnitude relative to the wild-type constructs and are rate-limiting in the ATPase cycles when micromolar substrate is used. The hydrolysis steps of E476K (at 4 °C) and E459V (at 20 °C) are slowed to such an extent that the proteins form ATP-bound complexes that are stable on the order of hours.

On and Off Rate Constants for Nucleotide Binding. The mantADP off rate constants for both E476K and E459V were reduced by about an order of magnitude but were much faster than the hydrolysis steps (Table 1). These off rate constants were measured by chasing mantADP from the protein in two ways. The first was to chase protein-bound mantADP after it had been created by the hydrolysis of mantATP on the

protein (Figure 3). The second was to simply bind mantADP to the protein and then chase it off. Both experiments gave similar results for M761-2R (1.5 s^{-1}), E476K (0.2 s^{-1}), and E459V (0.05 s^{-1}).

The mantATP on rate constants of the proteins were easily obtained and found to be similar (Table 1). The extremely slow rate of the hydrolysis step of E459V allowed for a direct measurement of the ATP off rate constant, and was found to be 2×10^{-5} s^{-1}. A number of groups have calculated the ATP off rate constant from rabbit S-1 through measurements of other rate constants of the ATPase cycle, and a range of values has been reported: 1.6×10^{-3} to 2×10^{-7} s^{-1} (*29*−*32*). Their calculations were necessarily more involved than the current measurement because the hydrolysis step is rapid in S-1. The K_d for mantATP binding to E459V is calculated as $k_{off}/k_{on} = 0.3$ nM (Table 1), which is compatible with estimates for the mammalian muscle myosin (*32*, *33*). This suggests that the recognition of ATP by *Dictyostelium* myosin and the E459V mutant is similar to the well-characterized mammalian myosin.

The use of E459V also clearly demonstrates that actin can accelerate the release of ATP from the myosin·ATP complex by 100-fold and probably by at least 1000-fold at saturating actin concentrations (*34*, *35*). This is required in mammalian myosin by detailed balance as ATP reduces the affinity of myosin for actin by at least 1000-fold. The actin-induced dissociation of the myosin·mantATP complex (Figure 5A, filled arrow) and the ATP-induced dissociation of the actomyosin complex (Figure 6B, open arrow) demonstrate that myosin will bind either substrate tightly if one is in excess over the other.

Actin Binding. The second-order rate constant of ATP-induced actomyosin dissociation is about an order of magnitude larger for E459V than for M761-2R. This enhancement was also seen in experiments on M754 by Woodward et al. (*36*). Pyrene-actin titration experiments showed that nucleotide-free E459V binds actin filaments with a K_d of $\ll 1$ μM, as does M761-2R. By contrast, E476K does not bind actin at micromolar concentrations of the proteins as shown by titration and cosedimentation experiments. Under the conditions used, the actin binding interface of E476K may be uncoupled from changes that occur at the nucleotide binding site, and remain permanently in a low actin affinity conformation.

Importance of the Mutated Residues. The mutations that were investigated are positioned within a highly conserved loop−helix structure which contains the loop that is commonly referred to as switch II (*37*). It has been suggested that this loop−helix structure might help communicate conformational changes at the nucleotide binding pocket to both the putative lever-arm and the actin binding site (*38*). Our results demonstrate that the ATPase cycle of either mutant is dominated by the ATP-bound state.

Why does the E459V mutation greatly reduce the hydrolysis step? Switch II (residues G457 to S465 in the *D. discoideum* sequence) is probably important for nucleotide triphosphate hydrolysis by myosin, kinesin, and a number of G-proteins (*37*, *39*). E459 and G457 are within switch II and are present in the γ-phosphate pocket of the vanadate·ADP·S1Dc structure which was interpreted as a model of the transition state of myosin (*14*). It has been suggested that residues E459 and G457 play an important role in positioning and polarizing a water molecule for attack on the γ-phosphate (*14*, *40*). In the E459V mutation, the charged oxygen of the glutamic acid residue is no longer available to participate in this interaction (*40*). Onishi et al. (*41*) found that the mutation E459A made in chicken smooth muscle heavy meromyosin reduced the basal ATPase rate by at least 1 order of magnitude and eliminated the P_i burst. They concluded that the rate of the hydrolysis step was greatly reduced but did not report the actual amount that the step was reduced relative to their wild-type construct. In the present experiments, the glutamic acid residue was replaced by a valine, and the hydrolysis step was reduced by 6 orders of magnitude.

Many structural techniques require a protein conformation be essentially static on the minutes time-scale, and therefore E459V provides an excellent starting point for investigating the differences between the apo- and ATP-bound states. The E459V structures may help test whether the reversal of the lever arm swing accompanies the actomyosin to myosin·ATP transition (*4*, *5*). Also, a single preparation could be used to reveal the time-dependent structural changes that occur when myosin·ATP evolves to myosin·ADP.

E476 is not part of the nucleotide binding pocket but positioned in the center of the switch II helix, where it forms part of a communication path that links the nucleotide binding and actin binding sites. Residues I514, H572, and Y573, which are important in positioning the actin binding region formed by residues 518−568 on the surface of the myosin motor, are located only ~5 Å away from E476. Two of these residues, H572 and Y573, are part of the HYAG motif, a highly conserved sequence motif that is found in myosins from all classes. Substitution of E476 with a glutamine instead of a lysine results in uncoupling of solution-activated ATPase activity from in vitro motility (*13*). As mentioned above, the surprising feature is that the actin binding interface of M761-1R with the E476K mutation remains in a low actin affinity state. Thus, the structure of actin binding interface of this mutant compared to M761-1R will be of interest since current crystal structures give little information on how the binding of ATP to myosin heads results in a >3 order of magnitude reduction in actin affinity.

In summary, we have generated and characterized myosin head fragments that are greatly slowed at the ATP hydrolysis step, and used one of the constructs to make a direct measurement of the ATP off rate constant. M761-1R with the mutation E459V hydrolyzes ATP on the hours time-scale at 20 °C and thus forms a stable ATP complex relative to the time necessary to gather structural data. Thus, structural analyses of E476K and E459V may elucidate key structural features of the myosin ATPase cycle. The ATP off rate constant was obtained with the E459V construct, and could be accelerated by at least 100-fold by actin. The K_d for ATP binding was obtained by direct measurements. It is compatible with values estimated from mammalian muscle myosin which suggests that the recognition of ATP by *Dictyostelium* and mammalian myosin is similar.

ACKNOWLEDGMENT

We thank A. Spudich for help and discussions; H. Warrick and S. Zimmermann for help with DNA constructs; M. L. W. Knetsch, M. Furch, and N. Adamek for help with early

experiments; T. Pollard for kindly providing the M2.42 antibody; and J. Lorsch, P. O'Brien, and D. N. Robinson for useful comments on the manuscript.

REFERENCES

1. De Lozanne, A., and Spudich, J. A. (1987) *Science 236*, 1086−1091.
2. Pasternak, C., Spudich, J. A., and Elson, E. L. (1989) *Nature 341*, 549−551.
3. Lymn, R. W., and Taylor, E. W. (1971) *Biochemistry 10*, 4617−4624.
4. Eisenberg, E., and Greene, L. E. (1980) *Annu. Rev. Physiol. 42*, 293−309.
5. Geeves, M. A., Goody, R. S., and Gutfreund, H. (1984) *J. Muscle Res. Cell Motil. 5*, 351−361.
6. Rayment, I., Rypniewski, W. R., Schmidt-Bäase, K., Smith, R., Tomchick, D. R., Benning, M. M., Winkelmann, D. A., Wesenberg, G., and Holden, H. M. (1993) *Science 261*, 50−58.
7. Irving, M., Lombardi, V., Piazzesi, G., and Ferenczi, M. A. (1992) *Nature 357*, 156−158.
8. Irving, M., St Claire Allen, T., Sabido-David, C., Craik, J. S., Brandmeier, B., Kendrick-Jones, J., Corrie, J. E., Trentham, D. R., and Goldman, Y. E. (1995) *Nature 375*, 688−691.
9. Thomas, D. D., Ramachandran, S., Roopnarine, O., Hayden, D. W., and Ostap, E. M. (1995) *Biophys. J. 68*, 135S−141S.
10. Whittaker, M., Wilson-Kubalek, E. M., Smith, J. E., Faust, L., Milligan, R. A., and Sweeney, H. L. (1995) *Nature 378*, 748−751.
11. Anson, M., Geeves, M. A., Kurzawa, S. E., and Manstein, D. J. (1996) *EMBO J. 15*, 6069−6074.
12. Uyeda, T. Q., Abramson, P. D., and Spudich, J. A. (1996) *Proc. Natl. Acad. Sci. U.S.A. 93*, 4459−4464.
13. Ruppel, K. M., and Spudich, J. A. (1996) *Mol. Biol. Cell 7*, 1123−1136.
14. Smith, C. A., and Rayment, I. (1996) *Biochemistry 35*, 5404−5417.
15. Fisher, A. J., Smith, C. A., Thoden, J. B., Smith, R., Sutoh, K., Holden, H. M., and Rayment, I. (1995) *Biochemistry 34*, 8960−8972.
16. Smith, C. A., and Rayment, I. (1995) *Biochemistry 34*, 8973−8981.
17. Gulick, A. M., Bauer, C. B., Thoden, J. B., and Rayment, I. (1997) *Biochemistry 36*, 11619−11628.
18. Kuczmarski, E. R., and Spudich, J. A. (1980) *Proc. Natl. Acad. Sci. U.S.A. 77*, 7292−7296.
19. Kurzawa, S. E., Manstein, D. J., and Geeves, M. A. (1997) *Biochemistry 36*, 317−323.
20. Manstein, D. J., and Hunt, D. M. (1995) *J. Muscle Res. Cell Motil. 16*, 325−332.
21. Pardee, J. D., and Spudich, J. A. (1982) *Methods Cell Biol. 24*, 271−789.
22. Criddle, A. H., Geeves, M. A., and Jeffries, T. (1985) *Biochem. J. 232*, 343−349.
23. Hiratsuka, T. (1983) *Biochim. Biophys. Acta 742*, 496−508.
24. Woodward, S. K., Eccleston, J. F., and Geeves, M. A. (1991) *Biochemistry 30*, 422−430.
25. Ritchie, M. D., Geeves, M. A., Woodward, S. K., and Manstein, D. J. (1993) *Proc. Natl. Acad. Sci. U.S.A. 90*, 8619−8623.
26. Bagshaw, C. R., and Trentham, D. R. (1973) *Biochem. J. 133-(2)*, 323−328.
27. Barman, T. E., Hillaire, D., and Travers F. (1983) *Biochem. J. 209(3)*, 617−626.
28. Kouyama, T., and Mihashi, K. (1981) *Eur. J. Biochem. 114*, 33−38.
29. Mannherz, H. G., Schenck, H., and Goody, R. S. (1974) *Eur. J. Biochem. 48*, 287−295.
30. Wolcott, R. G., and Boyer, P. D. (1974) *Biochem. Biophys. Res. Commun. 57(3)*, 709−716.
31. Mannherz, H. G., and Goody, R. S. (1976) *Annu. Rev. Biochem. 45*, 427−465.
32. Goody, R. S., Hofmann, W., and Mannherz, H. G. (1977) *Eur. J. Biochem. 78(2)*, 317−324.
33. Taylor, E. M (1979) *CRC Crit. Rev. Biochem. 6(2)*, 103−164.
34. Houadjeto, M., Travers, F., and Barman, T. (1992) *Biochemistry 31*, 1564−1569.
35. Herrman, C., Houadjeto, M., Travers, F., and Barman, T. (1992) *Biochemistry 31*, 8036−8042.
36. Woodward, S. K. A., Geeves, M. A., and Manstein, D. J. (1995) *Biochemistry 34*, 16056−16064.
37. Smith, C. A., and Rayment, I. (1996) *Biophys. J. 70*, 1590−1602.
38. Cooke, R. (1997) *Physiol. Rev. 77(3)*, 671−697.
39. Vale, R. D. (1996) *J. Cell Biol. 135 (2)*, 291−302.
40. Holmes, K. C. (1996) *Curr. Opin. Struct. Biol. 6*, 781−789.
41. Onishi, H., Morales, M. F., Kojima, S., Katoh, K., and Fujiwara, K. (1997) *Biochemistry 36*, 3767−3772.

BI973143F